Fractional Order Adaptive Sliding Mode Control for the Deployment of Space Tethered System With Input Limitation

XIAOQING ZHONG[1], XIANGYU SHAO[2], (Student Member, IEEE),
XIAOLEI LI[2], (Student Member, IEEE), ZHIQIANG MA[2], (Student Member, IEEE),
AND GUANGHUI SUN [2], (Member, IEEE)
[1]Institute of Telecommunication Satellite, China Academy of Space Technology, Beijing 100094, China
[2]Research Institute of Intelligent Control and Systems, Harbin Institute of Technology, Harbin 150001, China

Corresponding author: Guanghui Sun (guanghuisun@ hit.edu.cn)

ABSTRACT This paper develops a novel sliding mode control strategy for the deployment of space tethered system with consideration of constrained input. The simplified nonlinear dynamic model of space tethered system in elliptical orbits is first modeled by using the Euler–Lagrange mechanical equation. Considering the flexibility of tether, the compression or any component of shear forces for the tether is assumed to be input limitation. By introducing fractional order operator and saturation function into the sliding surface, a new adaptive fractional order sliding mode control strategy is introduced based on the proposed nonlinear dynamic model. Compared with classical sliding mode methods, a faster deployment time without overshoot and chattering-reduced performance can be achieved. Finally, numerical simulations are illustrated to validate the effectiveness of our methods.

INDEX TERMS Dynamic sliding mode, elliptical orbits, fractional order sliding mode, input limitation, space tethered system.

I. INTRODUCTION

The Space Tethered System (STS), which is composed of space tethers and equipment such as satellites, space stations or space manipulators [1], [2], can terrifically expand the operation area of the space vehicle making use of the tether. The STS is applicable to many space tasks such as orbital transfer [3], debris removal [4], deep-space exploration [5] and etc [6]–[9]. Besides those theoretical researches, plenty of practical experiments, aiming to verify and evaluate the existing control methods, have been implemented by National Aeronautics and Space Administration (NASA) and European Space Agency (ESA) during the last decades [10], [11]. For every STS mission, a precondition is to deploy its tether to a desired position, which means that deployment is an essential operation. Moreover, it is fairly challenging to achieve stable and fast deployment due to the limited tension of the tether and thruster saturation [12], [13]. Therefore, researching the deployment process is worthy and significant.

In general, according to whether or not ancillary thrusters are installed on the subspacecraft, techniques to control the deployment process can be divided into two categories, namely, hybrid tension control and tension-only control. For instance, [14] investigated the tension-only deployment process and put forward an adaptive sliding mode control law with input limitation. Conversely, [15] studied tether deployment from a spool-type reel with assistant thrusters and carried out simulation and on-ground experiments. Owing to the weak coupling property of tether tension and out-of-plane angle, tension-only control scheme cannot regulate the out-of-plane angle effectively, which is a primary drawback of tension-only control [16]. On the contrary, there is no such problem in hybrid control which combines tension and thruster force [17]. Over and above that benefit, hybrid control can simplify the controller design and shorten mission executing time compared with tension-only control. Hence, in this paper, we will discuss the deployment of the STS with thrusters. On the other hand, how to use the thrusters properly to get ideal deployment dynamics is remaining to be solved. Thereby, to achieve better deployment performance, many control methods such as sliding mode control, robust control [18], feedback linearization [19]

and backstepping control [20] are brought into hybrid tension control.

Among those above control methods, sliding mode control is famous for its superiority in handling uncertainties or disturbances [21]–[23]. Apart from high robustness, algorithm of sliding mode control is relatively straightforward, which is good for physical implementation. These above merits lead to wide use of sliding mode control in STS. For example, [24] investigated the deployment problem of short space tethered system and proposed a sliding mode control law. In order to approach the target with desired attitude, [25] came up with a coordinated control strategy which combined sliding mode control and optimal control. With the purpose of further improving the performance of sliding mode control, many methods such as observer-based method and state-dependent gain method are developed [26]. Besides, fractional order sliding mode control is also effective to meliorate the performance. This control scheme shows fascinating features like a decrease in the overshoot and the settling time [27]–[29]. However, only a few researchers tried applying it to STS. [30] applied fractional order sliding mode control strategy on the STS. Researchers may be inspired by his attempt. And moreover, they took external disturbance and unmodeled dynamics into account. In this literature, fractional order sliding mode control exhibited its strong ability in suppressing disturbance, reducing settling time and maximum overshoot. However, in the existing researches, there are three main problems remaining to be solved.

The first one is input limitation. Tension limitation and thruster saturation are inevitable when the designed control schemes applied in reality, which could cause undesired control results or even concussive system states if no special measures are taken to dispose of these constraints [31]. For example, during TSS-1R mission the tether broke because of the poor consideration of tension limitation [32]. Another problem is that most of the previous controllers are designed based on the linear dynamic model of STS, which may lead to poor control performance or even control system failure owing to the local linearizing the dynamic model in the neighborhood of the equilibrium point. Finally, most current controllers were designed based on systems in circular orbits while in reality elliptical orbits are more common. As a result, the difference between elliptical orbits and circular orbits could pose a negative effect on the control performance when it is put into practical applications. Hence, a controller to deal with nonlinear dynamic model that is established on elliptical orbits can achieve better performance in real world. However, as far as we known, there are few works have been done in this field.

In this paper, to deal with the above problems, a novel fractional order sliding mode control scheme based on nonlinear mathematical model in elliptical orbits is presented. A new dimensionless transform based on coordinate translation is constructed to convert input limitation into the form of saturation. With the help of this transform and Euler-Lagrange mechanical equation, dynamic model of STS deployment in elliptical orbits is established. In order to tackle tether tension limitation and thruster saturation, we introduce a quasi-saturated function and a bounded function, with their properties discussed completely. Furthermore, a fractional order sliding surface is constructed by bringing in fractional order derivative operator, reaching higher robustness, smaller overshoots and shorter settling time. Moreover, we design the controller according to the nonlinear dynamic model, which is a progress than linearized one. Simulation results are presented to evaluate the performance of the proposed methods. To the best of our knowledge, it is the first time in the literature that tether tension limitation and thruster saturation have been considered and handled for nonlinear model in elliptical orbits using a fractional order sliding mode controller simultaneously.

The paper consists of five sections. The nonlinear mathematical model of the STS deployment in elliptical orbits is established in Section II. In Section III, the fractional order adaptive sliding mode control law subject to input limitation is presented and asymptotic stability is proved with the help of Control Lyapunov Function. Section IV exhibits the simulations which evaluate the effectiveness and efficiency of the control algorithm. Conclusions are given in Section V.

II. MATHEMATICAL MODEL

As shown in Figure 1, the considered STS is composed of a mother satellite, a subsatellite and a tether. To establish the dynamic equations of the deployment process, two coordinate systems are introduced at first. O is located at the earth center. Coordinate O_1xyz stands for the orbital coordinate system, with the origin at centroid of STS. The directions of axes are specified as follows: O_1x and O_1z point to the moving forward direction of the orbit and the core of the earth downward, respectively. According to the right-hand rule, one can define axis O_1y. The other coordinate system $O_1x'y'z'$ is the body frame of the STS, which means that the origin of $O_1x'y'z'$ is the same as that of O_1xyz. O_1z' is collinear with the tether direction, pointing to subsatellite. $O_1x'y'z'$ can be obtained via coordinate rotation of O_1xyz around the fixed origin O_1, that is, O_1x' can be obtained by rotating O_1x along O_1y by angle θ and O_1y' can be acquired by rotating O_1y along O_1x by angle ϕ.
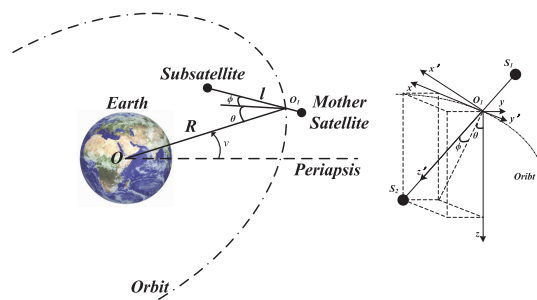

FIGURE 1. STS geometric representation.

Following assumptions are made, which can help reduce the complexity of derivation. Furthermore, these assumptions are reasonable, without losing key features and generality of the STS.

Assumption 1: The satellites of the STS are taken as non-volumetric particles without consideration of their attitude variations because during the deployment the tether is practically long enough. Take the earth as a perfect sphere so that the centroid of the earth coincides with the center of it.

Assumption 2: The orbit of the STS is elliptical.

Assumption 3: The mass of the mother satellite is considerably larger compared to that of the subsatellite. When the mass ratio of mother satellite to subsatellite is not less than 100, we think that the mother satellite is able to keep the nominal orbit and it is not affected by the subsatellite during the deployment task.

Assumption 4 [33]: The tether is springless and massless. Furthermore, it is considered as a rigid rod during the deployment, which is referred as the dumbbell model with three degrees of freedom.

Remark 1: In Assumption 4, the tether is regard as a rod. However, it is apparent that a rod can provide both normal force and tension while tension is the only force tether can offer. Therefore, one knows that the tether must be stretched during the deployment mission, which means that the tether tension should fulfill equation $\tau_t > 0$. $\tau_t = 0$ implies that the tether is loose and contradictory with the dumbbell model. Hence, a small positive number τ_{tmin} is given to denote the minimum tether tension to assure that the tether is stretched. On the other hand, the maximum tension provided by the tether is limited, which can be denoted by τ_{tmax}. Once $\tau_t > \tau_{tmax}$, the tether would break which will make the control of the STS fail. In summary, τ_t is bounded by two positive values, whose lower bound and upper bound are τ_{tmin} and τ_{tmax}, respectively.

Before giving out deduction of dynamics of deployment, some preliminary notations are exhibited in advance. R represents the instantaneous distance of OO_1. The coefficient of the earth gravity field and the true anomaly measured from periapsis are denoted as μ_e and f, respectively. Define the symbols m_1 and m_2 as the mass of the mother satellite and the subsatellite, respectively. As a result, $m = m_1 + m_2$ corresponds to the total mass of the STS. The remaining symbols are the state variables of the STS, with l representing the tether length between the two satellites, θ being the in-plane angle and ϕ indicating the out-of-plane angle, respectively. L stands for the total length of the tether. In this paper,

we use notation $(\dot{\cdot})$ to represent the time derivative of first order. Based on above assumptions and notations, one has the equations of kinetic energy and potential energy during the deployment established as follows [34], [35]:

$$T = \frac{1}{2}m(\dot{R}^2 + R^2\dot{f}^2) + \frac{1}{2}\bar{m}l^2\left[\dot{\phi}^2 + (\dot{\theta}+\dot{f})^2\cos^2\phi\right] + \frac{1}{2}\bar{m}\dot{l}^2 \tag{1}$$

$$V = -\frac{\mu_e m}{R} + \frac{\mu_e \bar{m}l^2}{2R^3}(1 - 3\cos^2\theta\cos^2\phi), \tag{2}$$

where $\bar{m} = m_1 m_2/m$.

Then apply Lagrangian mechanics theory, we can get Eq. (3), as shown at the bottom of this page, where $k = 1 + e\cos f$, e is the eccentricity of the Keplerian orbit, τ_t means the tether tension while τ_θ and τ_ϕ represent thruster torques affecting in-plane angle and out-of-plane angle, respectively. τ_{td}, $\tau_{\theta d}$ and $\tau_{\phi d}$ are the external distrubances and they are assumed to be bounded. It is notable that tether tension τ_t is positive whereas thruster torques τ_θ and τ_ϕ have no such limitation, increasing the complexity for the controller design. To reduce the difficulty of designing a saturated controller, a novel dimensionless conversion is presented as follows [14]

$$\lambda = l/L$$
$$d()/dt = \dot{f}d()/df$$
$$\hat{\tau}_t = -\tau_t/(\bar{m}\dot{f}^2 L) + \rho$$
$$\hat{\tau}_\theta = \tau_\theta/(\bar{m}\dot{f}^2 L^2)$$
$$\hat{\tau}_\phi = \tau_\phi/(\bar{m}\dot{f}^2 L^2)$$
$$\hat{\tau}_{td} = \tau_{td}/(\bar{m}\dot{f}^2 L)$$
$$\hat{\tau}_{\theta d} = \tau_{\theta d}/(\bar{m}\dot{f}^2 L^2)$$
$$\hat{\tau}_{\phi d} = \tau_{\phi d}/(\bar{m}\dot{f}^2 L^2), \tag{4}$$

in which ρ is a positive number. According to Eq. (4), proper ρ can be selected such that $\hat{\tau}_{tmin} < 0$ and $\hat{\tau}_{tmax} > 0$. Thus, $\hat{\tau}_t$, $\hat{\tau}_\theta$ and $\hat{\tau}_\phi$ are transformed into the unified form. Based on transformation in Eq. (4), one can convert Eq. (3) into dimensionless Euler-Lagrange dynamical equation shown below:

$$H(q)\ddot{q} + C(q,\dot{q})\dot{q} + B_0\dot{q} + G(q) = \tau + \tau_d, \tag{5}$$

where

$$q = \begin{pmatrix} \lambda & \theta & \phi \end{pmatrix}^T$$
$$\tau = \begin{pmatrix} \hat{\tau}_t & \hat{\tau}_\theta & \hat{\tau}_\phi \end{pmatrix}^T$$
$$H(q) = \begin{bmatrix} 1 & 0 & 0 \\ 0 & \lambda^2\cos^2\phi & 0 \\ 0 & 0 & \lambda^2 \end{bmatrix}$$

$$\bar{m}\ddot{l} - \frac{2e\sin f}{k}\dot{l}f - \bar{m}l\left[\dot{\phi}^2 + (\dot{\theta}+\dot{f})^2\cos^2\phi\right] + \frac{\bar{m}l\dot{f}^2}{k}(1 - 3\cos^2\phi\cos^2\theta) = -\tau_t + \tau_{td}$$

$$\bar{m}l^2\cos^2\phi\ddot{\theta} - \frac{2e\sin f}{k}\dot{\theta}fl^2\cos^2\phi - \frac{2e\sin f}{k}\dot{\theta}f^2l^2\cos^2\phi + 2\bar{m}(\dot{\theta}+\dot{f})l^2\cos^2\phi\left(\frac{\dot{l}}{l} - \dot{\phi}\tan\phi\right) + \frac{3}{k}\bar{m}\dot{f}^2l^2\sin\theta\cos\theta\cos^2\phi = \tau_\theta + \tau_{\theta d}$$

$$\bar{m}l^2\ddot{\phi} - \frac{2e\sin f}{k}\dot{\phi}fl^2 + 2\bar{m}\dot{\phi}\dot{l}l + \bar{m}l^2\sin\phi\cos\phi\left[(\dot{\theta}+\dot{f})^2 + 3\bar{m}\dot{f}\cos^2\theta\right] = \tau_\phi + \tau_{\phi d} \tag{3}$$

$$C(q, \dot{q}) = \begin{bmatrix} C_1 & C_2 & C_3 \end{bmatrix}$$

$$B_0 = \begin{bmatrix} -\dfrac{2e\sin f}{k} & 0 & 0 \\ 0 & -\dfrac{2e\sin f}{k} & 0 \\ 0 & 0 & -\dfrac{2e\sin f}{k} \end{bmatrix} \quad (6)$$

$$G(q) = \begin{bmatrix} -\lambda\cos^2\phi + \dfrac{\lambda}{k}(1 - 3\cos^2\theta\cos^2\phi) + \rho \\ \dfrac{3}{k}\lambda^2\cos\theta\sin\theta\cos^2\phi - \dfrac{2e\sin f}{k} \\ (\lambda^2 + \dfrac{3}{k}\lambda^2\cos^2\theta)\sin\phi\cos\phi \end{bmatrix}$$

$$C_1 = \begin{bmatrix} 0 \\ (2\lambda + \lambda\dot{\theta})\cos^2\phi \\ \lambda\dot{\phi} \end{bmatrix}$$

$$C_2 = \begin{bmatrix} -(\lambda\dot{\theta} + 2\lambda)\cos^2\phi \\ \lambda\dot{\lambda}\cos^2\phi - \lambda^2\dot{\phi}\sin\phi\cos\phi \\ \lambda^2(\dot{\theta} + 2)\sin\phi\cos\phi \end{bmatrix}$$

$$C_3 = \begin{bmatrix} -\lambda\dot{\phi} \\ -(\dot{\theta} + 2)\lambda^2\sin\phi\cos\phi \\ \lambda\dot{\lambda} \end{bmatrix}.$$

It is obvious that $\dot{H}(q) - 2C(q, \dot{q})$ is skew-symmetric, leading to

$$q^T(\dot{H}(q) - 2C(q, \dot{q}))q = 0. \quad (7)$$

Remark 2: B_0 represents a diagonal non-positive definite matrix related to elliptical orbit and it is clear that B_0 is determined by orbital eccentricity e and true anomaly f. According to the definition of ellipse and celestial kinematics, e is limited in a region $[0, e_0]$ where $e_0 < 1$. Similarly, $\sin f$ is bounded. Thus, we can prove that B_0 is bounded too and denote its upper bound as φ_2 which satisfies $\|B_0\| < \varphi_2$.

Remark 3: Denote the maximum dimensionless tether length ratio as λ_{max}. Similar to Remark 1, the dimensionless tether length cannot be zero. Once $\lambda = 0$ sets up, it means that two satellites of the STS come into collision with each other, which is not permitted during the deployment mission. Even worse, the dimensionless conversion is singular if $\lambda = 0$ establishes. To avoid the problems mentioned above, denotation λ_{min} is brought in, such that

$$0 < \lambda_{min} \le \lambda \le \lambda_{max}. \quad (8)$$

III. FRACTIONAL ORDER SLIDING MODE CONTROL

In this section, the control law for STS taking advantage of fractional order sliding mode control is presented based on the dynamic model established in the previous section. Some requisite preliminaries and properties are shown at first for the subsequent derivation.

A. PRELIMINARIES

The general torques in the Euler-Lagrange dynamic equation expressed by Eq. (5) can be parameterized as the expression $Z(q, \dot{q}, \dot{q}, \ddot{q})\Theta = \tau$, in which $Z(q, \dot{q}, \dot{q}, \ddot{q})$ is a function made up of known nonlinear functions and Θ is a dimensionless

vector constituting unknown but constant parameters [36]. Substituting a nominal reference $\dot{q}_r$ into Eq. (5), one has:

$$H(q)\ddot{q}_r + C(q, \dot{q})\dot{q}_r + B_0\dot{q}_r + G(q) = Z_r\Theta, \quad (9)$$

where $Z_r = Z_r(q, \dot{q}, \dot{q}_r, \ddot{q}_r)$. Construct the open-loop error dynamics S_r as follows:

$$S_r = \dot{q} - \dot{q}_r. \quad (10)$$

Consider Eq. (5) and Eq. (9) simultaneously, one gets:

$$H(q)\dot{S}_r + C(q, \dot{q})S_r + B_0S_r = \tau + \tau_d - Z_r\Theta. \quad (11)$$

Properties 1 [37]: One can always find positive scalars $\delta_i(i = 0, \ldots, 5)$ such that

$$\|H(q)\| \ge \lambda_{min}(H(q)) > \delta_0 > 0$$
$$\|H(q)\| \le \lambda_{max}(H(q)) < \delta_1 < \infty$$
$$\|C(q, \dot{q})\| \le \delta_2\|\dot{q}\|$$
$$\|G(q)\| \le \delta_3$$
$$\|\dot{q}_r\| \le \delta_4 + \alpha\|\Delta q\| + \beta\|\sigma\|$$
$$\|\ddot{q}_r\| \le \delta_5 + \alpha\|\Delta\dot{q}\|, \quad (12)$$

where $\lambda_{min}(\cdot)$ and $\lambda_{max}(\cdot)$ stand for the minimum and maximum eigenvalues of matrix, respectively. We assume that all the states of the STS are bounded, which always holds in practice. In addition, $Z_r\Theta$ is considered bounded such that $Z_r\Theta \le \eta(t)$ because a bounded function $\eta(t) = f(\Delta q, \Delta\dot{q}, \sigma, \delta_i, t)$ which depends on system states can always be found. We define φ_0 as the bound of $\eta(t)$ such that $|\eta(t)| \le \varphi_0$, which represents uncertainty of the system.

In order to deal with the saturation phenomenon, several definitions and comments are brought in.

Definition 1: Define a quasi-saturated function:

$$Qsat(x) = \begin{cases} sign(x) & |x| \ge \pi/2 \\ sin(x) & |x| < \pi/2 \end{cases}. \quad (13)$$

Remark 4: Apparently, function $y = Qsat(x)$ is strictly bounded, or to be more precise, is saturated. In addition, according to Definition 1, function $y = Qsat(x)$ satisfies the equation $|Qsat(x)| \le |x|, \forall x$.

Remark 5 [38]: Utilizing the properties of function $y = Qsat(x)$ and $y = arcsin(x)$, one has

$$|Qsat(x) + \Delta h| \le |x + arcsin(\Delta h)| \quad (14)$$
$$sign(Qsat(x) + \Delta h) = sign(x + arcsin(\Delta h)), \quad \forall x, |\Delta h| < 1. \quad (15)$$

Definition 2 [39], [40]: Define a bounded function formed as follows:

$$\tau_{out}(x) = \begin{cases} x_{ub} & x > x_{ub} \\ x & x_{lb} \le x \le x_{ub} \\ x_{lb} & x < x_{lb} \end{cases}, \quad (16)$$

where x_{lb} and x_{ub} represent the minimum and maximum value of $\tau_{out}(x)$, respectively, and satisfy $x_{lb} < 0 < x_{ub}$.

Remark 6: According to the dimensionless transformation described by Eq. (4), the generalized tension and torques

in the channel of in-plane angle and out-of-plane angle are limited, which means that they are in the form of Eq. (16). Suppose $x = [x_1, x_2, \cdots, x_n]^T$. Then we define the following equations to specify function $\tau_{out}(x)$, $arcsin(x)$ and $sign(x)$ who use vectors as input parameters

$$\tau_{out}(x) = \begin{pmatrix} \tau_{out}(x_1) \\ \tau_{out}(x_2) \\ \cdots \\ \tau_{out}(x_n) \end{pmatrix} \tag{17}$$

$$arcsin(x) = \big(arcsin(x_1), arcsin(x_2), \cdots, arcsin(x_n)\big)^T \tag{18}$$

$$sign(x) = \big(sign(x_1), sign(x_2), \cdots, sign(x_n)\big)^T. \tag{19}$$

Remark 7: According to Eq. (16), the following relations hold

$$|\tau_{out}(x)| \leq |x|$$
$$sign(\tau_{out}(x)) = sign(x). \tag{20}$$

Introducing a new one dimension parameter J, one can rewrite Eq. (16) as shown below:

$$\tau_{out}(x) = Jx, \tag{21}$$

where J is a nonnegative scalar and the value of J is related to x. It is obvious that J is in the range of [0,1]. Furthermore, from Eq. (20), we can see that if the input variable x is bounded between x_{min} and x_{max}, $x_{min} < 0 < x_{max}$, then there always exists the lower bound of J such that

$$J_{lb} = min(x_{lb}/x_{min}, x_{ub}/x_{max}). \tag{22}$$

Assume $x = [x_1, x_2, \cdots, x_n]^T$ and all its elements are bounded. Following equations can be obtained using Eq. (20)

$$\tau_{out}(x_1) \geq J_{lb1}x_1$$
$$\tau_{out}(x_2) \geq J_{lb2}x_2$$
$$\vdots$$
$$\tau_{out}(x_n) \geq J_{lbn}x_n, \tag{23}$$

where $J_{lb1}, J_{lb2}, \cdots J_{lbn}$ are all positive numbers. Eq. (23) can be denoted in the following matrix form

$$\tau_{out}(x) \geq \begin{bmatrix} J_{lb1} & 0 & 0 \\ 0 & \ddots & 0 \\ 0 & 0 & J_{lbn} \end{bmatrix} x. \tag{24}$$

For briefness, denote that

$$J_m = \begin{bmatrix} J_{lb1} & 0 & 0 \\ 0 & \ddots & 0 \\ 0 & 0 & J_{lbn} \end{bmatrix}. \tag{25}$$

The aforementioned definitions and remarks present some characteristics of saturated functions, which works in the proof of stability. Before presenting the control law, for clarity, it is necessary to declare the fractional order operators and some routine lemmas in advance to support the derivation.

Definition 3 [27]: The Riemann-Liouville integral operator is formed as

$$_{t_0}I_t^v f(t) = \frac{1}{\Gamma(v)} \int_{t_0}^t \frac{f(\varsigma)}{(t-\varsigma)^{1-v}} d\varsigma. \tag{26}$$

Definition 4 [27]: The Riemann-Liouville derivative can be expressed by:

$$_{t_0}D_t^v f(t) = \frac{1}{\Gamma(m-v)} \frac{d^m}{dt^m} \int_{t_0}^t \frac{f(\varsigma)}{(t-\varsigma)^{v-m+1}} d\varsigma, \tag{27}$$

where $\Gamma(z) = \int_0^\infty t^{z-1}e^{-t}dt$ is gamma function, m is an integer such that $m-1 < v < m$.

Definition 5 [36] The Laplace Transform of Riemann-Liouville derivative can be calculated by the following expression:

$$\mathscr{L}\{_{t_0}D_t^v f(t)\} = s^v F(s) - \sum_{k=0}^{m-1} s^k {}_{t_0}D_t^{v-k-1}f(t)|_{t=t_0}. \tag{28}$$

Lemma 1 [36]: Consider a fractional order differential equation shown below:

$$\dot{x} + \alpha_{r-1}x^{((r-1)/r)} + \cdots + \alpha_0 = 0. \tag{29}$$

where r is a positive integer. Utilizing Definition 5 and transformation $|s| = |w|^r$, one has

$$w^r + \alpha_{r-1}w^{r-1} + \cdots + \alpha_0 = 0. \tag{30}$$

Then, the system is stable if

$$|arg(w)| \geq \pi/2r. \tag{31}$$

For better understanding, the relation between root location and state stability in complex plane is depicted in Figure 2.
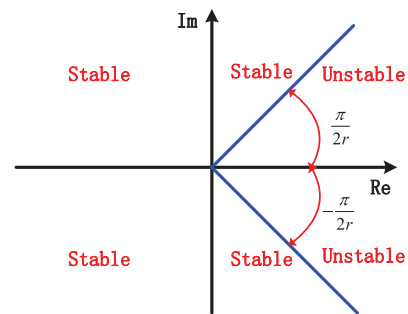

FIGURE 2. Stability regions of the fractional order system.

In the following, we define the exponential of matrix which is utilized in the control law.

Definition 6: The exponential of matrix $K \in R^{n \times n}$ is defined as:

$$e^K = \begin{bmatrix} e^{K_{11}} & \cdots & e^{K_{1n}} \\ \vdots & & \vdots \\ e^{K_{n1}} & \cdots & e^{K_{nn}} \end{bmatrix}. \tag{32}$$

When the STS is orbiting in an elliptical orbit, there are external disturbances caused by gravity gradient, aerodynamic drag and the irregularity of the earth. If not take into consideration, the external disturbances can cause negative

effects on the controllers. In order to make our simulations closer to the reality, an assumption on disturbances is given below.

Assumption 5: According to [41], the magnitude of the total disturbance torque is in the range of 1×10^{-5} and its period equals the orbital period T_0. T_0 can be obtained by following equations

$$T_0 = 2\pi/\Omega$$
$$\Omega = \sqrt{\mu_e/a^3}. \tag{33}$$

Hence, external disturbance after dimensionless transformation is acquired

$$\tau_d = [1.745 \times 10^{-4} \sin f, 4.985$$
$$\times 10^{-8} \sin f, \cdots 4.985 \times 10^{-8} \sin f]^T. \tag{34}$$

where the orbital parameters are shown in Case 1 in Section IV. However, the magnitude of τ_d is rather small. In order to examine the disturbance resisting ability of our controllers, we employ τ_d with greater amplitude as

$$\tau_d = [5 \times 10^{-2} \sin f, 5 \times 10^{-2} \sin f, 5 \times 10^{-2} \sin f]^T. \tag{35}$$

In addition, the disturbance is assumed to be bounded such that $\|\hat{\tau}_d\| \le \varphi_3 < \infty$, where φ_3 stands for the bound of the disturbance and it is chosen as $\varphi_3 = 0.1$.

B. FRACTIONAL ORDER ADAPTIVE SLIDING MODE CONTROL SUBJECT TO INPUT LIMITATION

Compared with conventional sliding mode control scheme or conventional dynamic sliding PID control, fractional order sliding mode control subject to input limitation can achieve less stabilization time with smaller overshoot. For improving the performance of the sliding mode dynamics, the fractional order sliding surface with the nature of memory and heritage is introduced in this subsection [42]. Furthermore, this solution is able to tackle the input limitation problem.

Based on the above knowledge, the fractional order adaptive sliding mode control with constrained input can be realized by the subsequent theorem.

Theorem 1 (Fractional Order Adaptive Sliding Mode Control Subject to Input Limitation): For stabilizing the dynamics of the deployment of the STS in Eq. (11), construct the fractional order adaptive sliding mode control input

$$\tau = -\tau_{out}(\zeta\varphi_1\vartheta_1 sign(S_{r1}) + \zeta\varphi_2\vartheta_2 S_{r2}), \tag{36}$$

where

$$S_{r1} = S_{q1} + \gamma \int_{t_0}^{t} S_{q1}(\varsigma)d\varsigma$$
$$S_{q1} = Qsat(\Delta\dot{q} + \alpha_0\Delta q + \alpha_1 D^\nu \Delta q), \tag{37}$$

in which, $\vartheta_1(0) > 0$, $\vartheta_2(0) > 0$, and the derivatives of ϑ_1 and ϑ_2 can be calculated by:

$$\dot{\vartheta}_1 = \zeta\varphi_1 S_{r2}^T K_1 e^{-2K_1^{-1}\vartheta_1^{-1}} sign(S_{r2})$$
$$- K_1 e^{K_1^{-1}\vartheta_1^{-1}}(\vartheta_1 - K_1^{-1})S_{r2}^T sign(S_{r2})$$

$$\dot{\vartheta}_2 = \zeta\varphi_2 S_{r2}^T K_1 e^{-2K_1^{-1}\vartheta_2^{-1}} S_{r2}$$
$$- K_1 e^{K_1^{-1}\vartheta_1^{-1}}(\vartheta_2 - K_1^{-1})S_{r2}^T(S_{r2}), \tag{38}$$

where ν is the order of the fractional term $\alpha_1 D^\nu \Delta q$. Typically, ν is selected as $\nu = 0.5$ such that the dynamics is asymptotically stable. Δq is the system states error and can be expressed by $\Delta q = q - q_d$ where q_d is the reference trajectory. ζ is a design parameter specifying the dynamics of deployment, which is constrained by $\zeta > 1$. φ_1 stands for the bound of lumped uncertainty satisfying $\varphi_1 > \varphi_0 + \varphi_2 + \varphi_3$ and φ_2 is the upper bound of B_0 according to Remark 3. γ represents a positive definite diagonal coefficient matrix varying over time. Moreover, S_{q1} is bounded according Definition 1, or to be more exactly, saturated. Therefore one can have bounded S_{r_1} when the system states are well controlled.

Remark 8: In this control law, we adopt two adaptive items ϑ_1 and ϑ_2. ϑ_1 and ϑ_2 are delicately constructed so that they can eliminate the side-effect of input limitation and perturbations generated by elliptical orbits in the process of stability analysis, respectively. On the other hand, from the derivatives of the adaptive terms, we can see that they will remain stable at constant values when $S_{r2} = 0$. As a result, they can be used to reflect whether S_{r2} converges to zero.

Proof: Construct a dynamic coordinate change S_{r2} with the system state error Δq and inverse sine function $arcsin(x)$:

$$S_{r2} = S_{q2} + arcsin(\gamma \int_{t_0}^{t} S_{q1}(\varsigma)d\varsigma)$$
$$S_{q2} = \Delta\dot{q} + \alpha_0\Delta q + \alpha_1 D^\nu \Delta q. \tag{39}$$

Until now, we have established two sets of sliding mode manifolds, that is, manifold S_r which includes S_{r1} and S_{r2}, and sub-manifold S_q which includes S_{q1} and S_{q2}. It is kind of complicated to construct so many alike symbols but they are all helpful during the analysis of Lyapunov stability. The sliding surface $S_{r2} = 0$ is first reached under the designed control input τ and then based on the relationship between S_{r2} and S_{q2}, one can prove the asymptotic stability of S_{q2}. Finally, after reaching the sliding surface $S_{q2} = 0$, we are able to discuss the stability of the decayed system $\Delta\dot{q} = -\alpha_0\Delta q - \alpha_1 D^\nu \Delta q$. This is the main clue of the following proof.

As we know, the domain of definition of function $arcsin(x)$ is [-1,1]. To meet this demand, we can define γ as follows

$$\gamma = \begin{bmatrix} \gamma_1 & 0 & 0 \\ 0 & \gamma_2 & 0 \\ 0 & 0 & \gamma_3 \end{bmatrix}. \tag{40}$$

We can denote S_{q1} as $[S_{q1}^1, S_{q1}^2, S_{q1}^3]^T$ according to its definition. Then, for each parameter γ_i, the equation $\gamma_i \int_{t_0}^{t} S_{q1}^i(\varsigma)d\varsigma \in [-1, 1]$ must be fulfilled, where $i = 1, 2, 3$. Hence, we designed the adjustment law of γ_i as follows

$$\gamma_i = \begin{cases} \gamma_{i0} & \gamma_{i0}(|\int_{t_0}^{t} S_{q1}^i(\varsigma)d\varsigma|) \le 1 \\ c_i(|\int_{t_0}^{t} S_{q1}^i(\varsigma)d\varsigma|)^{-1} & \gamma_{i0}(|\int_{t_0}^{t} S_{q1}^i(\varsigma)d\varsigma|) > 1, \end{cases} \tag{41}$$

where γ_{i0} stands for the value of γ_i at the previous moment and c_i is a positive coefficient which satisfies $0 < c_i \le 1$.

According to Remark 5, it is apparent that S_{r2} and S_{r1} satisfy:

$$S_{r2}^T sign(S_{r2}) \geq S_{r1}^T sign(S_{r1}) \qquad (42)$$

$$sign(S_{r2}) = sign(S_{r1}). \qquad (43)$$

By introducing the limited input and substituting the dynamic coordinate change S_{r2} in Eq. (11) for S_r, one can get the below equation:

$$H(q)\dot{S}_{r2} = -\tau_{out}(\zeta\varphi\vartheta \, sign(S_{r1}) + \zeta\varphi_2\vartheta_2 S_{r2}) \\ + \tau_d - C(q,\dot{q})S_{r2} - B_0 S_{r2} - Z_{r2}\Theta. \qquad (44)$$

Define a positive definite Lyapunov function

$$V = \frac{1}{2}S_{r2}^T H(q)S_{r2} + \frac{1}{2}\tilde{\vartheta}_1^2 + \frac{1}{2}\tilde{\vartheta}_2^2, \qquad (45)$$

where $\tilde{\vartheta}_1 = \vartheta_1 \, e^{K_1^{-1}\vartheta_1^{-1}}$, $\tilde{\vartheta}_2 = \vartheta_2 \, e^{K_1^{-1}\vartheta_2^{-1}}$, and the time derivative of Lyapunov function V is expressed

$$\dot{V} = S_{r2}^T H(q)\dot{S}_{r2} + \frac{1}{2}S_{r2}^T \dot{H}(q)S_{r2} + \tilde{\vartheta}_1\dot{\tilde{\vartheta}}_1 + \tilde{\vartheta}_2\dot{\tilde{\vartheta}}_2$$
$$= -S_{r2}^T \tau_{out}(\zeta\varphi_1\vartheta_1 sign(S_{r1}) + \zeta\varphi_2\vartheta_2 S_{r2})$$
$$\quad - S_{r2}^T B_0 S_{r2} + \frac{1}{2}S_{r2}^T \dot{H}(q)S_{r2} - S_{r2}^T Z_{r2}\Theta$$
$$\quad - S_{r2}^T C(q,\dot{q})S_{r2} + \tilde{\vartheta}_1\dot{\tilde{\vartheta}}_1 + \tilde{\vartheta}_2\dot{\tilde{\vartheta}}_2 + S_{r2}^T \tau_d$$
$$= -S_{r2}^T \tau_{out}(\zeta\varphi_1\vartheta_1 sign(S_{r1}) + \zeta\varphi_2\vartheta_2 S_{r2})$$
$$\quad + \frac{1}{2}S_{r2}^T(\dot{H}(q) - 2C(q,\dot{q}))S_{r2} - S_{r2}^T B_0 S_{r2}$$
$$\quad - S_{r2}^T Z_{r2}\Theta + \tilde{\vartheta}_1\dot{\tilde{\vartheta}}_1 + \tilde{\vartheta}_2\dot{\tilde{\vartheta}}_2 + S_{r2}^T \tau_d. \qquad (46)$$

According to Eq. (7), it has

$$\dot{V} = -S_{r2}^T \tau_{out}(\zeta\varphi_1\vartheta_1 sign(S_{r1}) + \zeta\varphi_2\vartheta_2 S_{r2})$$
$$\quad - S_{r2}^T Z_{r2}\Theta - S_{r2}^T B_0 S_{r2} + \tilde{\vartheta}_1\dot{\tilde{\vartheta}}_1 + \tilde{\vartheta}_2\dot{\tilde{\vartheta}}_2 + S_{r2}^T \tau_d, \qquad (47)$$

$\tilde{\vartheta}_1\dot{\tilde{\vartheta}}_1$ and $\tilde{\vartheta}_2\dot{\tilde{\vartheta}}_2$ can be derived as follows:

$$\tilde{\vartheta}_1\dot{\tilde{\vartheta}}_1 = \zeta\varphi_1 S_{r2}^T K_1(\vartheta_1 - K_1^{-1})sign(S_{r2})$$
$$\quad - K_1 e^{3K_1^{-1}\vartheta_1^{-1}}(\vartheta_1 - K_1^{-1})^2 S_{r2}^T sign(S_{r2})$$
$$\tilde{\vartheta}_2\dot{\tilde{\vartheta}}_2 = \zeta\varphi_2 S_{r2}^T K_1(\vartheta_2 - K_1^{-1})S_{r2}$$
$$\quad - K_1 e^{3K_1^{-1}\vartheta_2^{-1}}(\vartheta_2 - K_1^{-1})^2 S_{r2}^T S_{r2}. \qquad (48)$$

Then, Eq. (46) can be simplified as follows

$$\dot{V} \leq -S_{r2}^T \tau_{out}(\zeta\varphi_1\vartheta_1 sign(S_{r1}) + \zeta\varphi_2\vartheta_2 S_{r2})$$
$$\quad - S_{r2}^T B_0 S_{r2} + \zeta\varphi_1 S_{r2}^T K_1(\vartheta_1 - K_1^{-1})sign(S_{r2})$$
$$\quad - S_{r2}^T Z_{r2}\Theta + \zeta\varphi_2 S_{r2}^T K_1(\vartheta_2 - K_1^{-1})S_{r2} + S_{r2}^T \tau_d. \qquad (49)$$

According to Eq. (43) and Eq. (21), one has

$$\dot{V} \leq -S_{r2}^T \tau_{out}(\zeta\varphi_1\vartheta_1 sign(S_{r2}) + \zeta\varphi_2\vartheta_2 S_{r2}) + S_{r2}^T \tau_d$$
$$\quad + K_1 S_{r2}^T(\zeta\varphi_1\vartheta_1 sign(S_{r1}) + \zeta\varphi_2\vartheta_2 S_{r2}) - S_{r2}^T B_0 S_{r2}$$
$$\quad - S_{r2}^T Z_{r2}\Theta - \zeta\varphi_1 S_{r2}^T sign(S_{r2}) - \zeta\varphi_2 S_{r2}^T S_{r2}. \qquad (50)$$

Since that the command input $\zeta\varphi_1\vartheta_1 \, sign(S_{r1}) + \zeta\varphi_2\vartheta_2 \, S_{r2}$ is bounded, then we can choose a positive scalar K_1 such that:

$$-S_{r2}^T \tau_{out}(\zeta\varphi_1\vartheta_1 sign(S_{r2}) + \zeta\varphi_2\vartheta_2 S_{r2}) \qquad (51)$$
$$\leq K_1 S_{r2}^T(\zeta\varphi_1\vartheta_1 sign(S_{r1}) + \zeta\varphi_2\vartheta_2 S_{r2}), \qquad (52)$$

Rewrite Eq. (50) as:

$$\dot{V} \leq S_{r2}^T(-B_0 - \zeta\varphi_2)S_{r2} - \zeta\varphi_1 S_{r2}^T sign(S_{r2})$$
$$\quad - S_{r2}^T Z_{r2}\Theta + S_{r2}^T \tau_d. \qquad (53)$$

Utilizing Remark 3, Eq. (53) can be simplified as:

$$\dot{V} \leq S_{r2}^T \varphi_2(1 - \zeta)S_{r2} - \zeta\varphi_1 S_{r2}^T sign(S_{r2})$$
$$\quad - S_{r2}^T Z_{r2}\Theta + S_{r2}^T \tau_d. \qquad (54)$$

If $\zeta > 1$, one has $1 - \zeta < 0$, so

$$\dot{V} \leq -\varphi_1\zeta S_{r2}^T sign(S_{r2}) - S_{r2}^T Z_{r2}\Theta + S_{r2}^T \tau_d$$
$$\quad \leq -\varphi_1\zeta S_{r2}^T sign(S_{r2}) + \varphi_0 S_{r2}^T sign(S_{r2}) + S_{r2}^T \varphi_3 sign(S_{r2})$$
$$\quad \leq -\varphi_1\zeta S_{r2}^T sign(S_{r2}) + (\varphi_0 + \varphi_3)S_{r2}^T sign(S_{r2})$$
$$\quad \leq \varphi_1(1 - \zeta)S_{r2}^T sign(S_{r2})$$
$$\quad \leq 0. \qquad (55)$$

Owing to the boundedness property of the expression above, a large enough ζ can be chosen such that $\dot{V} \leq 0$. According to Barbalat's theorem [43], it means that S_{r2} asymptotically converges to zero with a set of suitable design parameters. So the first-level sliding surface $S_{r2} = 0$ exists.

Using $S_{r2} = 0$, one has

$$S_{q2} = -arcsin(\gamma \int_{t_0}^t S_{q1}(\varsigma)d\varsigma). \qquad (56)$$

Select the Control Lyapunov Function candidate consisting of S_{q2}

$$V_1 = \frac{1}{2}S_{q2}^T S_{q2}. \qquad (57)$$

The time derivative is

$$\dot{V}_1 = S_{q2}^T \dot{S}_{q2}$$
$$= -\frac{S_{q2}^T \gamma S_{q1}}{\sqrt{1 - \|\gamma \int_{t_0}^t S_{q1}(\varsigma)d\varsigma\|^2}}$$
$$\leq -\frac{S_{q1}^T \gamma S_{q1}}{\sqrt{1 - \|\gamma \int_{t_0}^t S_{q1}(\varsigma)d\varsigma\|^2}} \leq 0, \qquad (58)$$

$\dot{V}_1 = 0$ iff $S_{q1} = 0$, namely, $S_{q2} = 0$. Therefore, we prove the asymptotic stability of Eq. (56), that is, $S_{q2} \to 0$ as $t \to \infty$. Based on this result, one has

$$\Delta\dot{q} = -\alpha_0\Delta q - \alpha_1 D^\nu \Delta q. \qquad (59)$$

Until now, from the point of view of the sliding mode control, we have explained the reaching phase by the above contents. Moreover, the sliding phase handles the whole dynamics Eq. (11), in other words, the stability of Eq. (59) results in the

asymptotic stability of the whole system. Selecting different design parameters α_0 and α_1 corresponds to critically damped response, over-damped response or under-damped response. Furthermore, suitable parameters can guarantee the asymptotic stability of Eq. (37). According to Definition 5, Laplace transform of Eq. (59) gives rise to

$$s + \alpha_1 s^{0.5} + \alpha_0 = 0. \tag{60}$$

Substituting $s = w^2$ yields

$$w^2 + \alpha_1 w + \alpha_0 = 0, \tag{61}$$

which implies $arg(s) = 2arg(w)$. Hence, we can conclude that Eq. (59) is stable if

$$|arg(w)| > \pi/4. \tag{62}$$

Thus, the parameters can be decided accordingly. This completes the proof. □

Remark 9: If $\alpha_1 = 0$, there is no fractional order differentiation on the sliding surface [38]. Therefore, we can call the decayed control law as traditional integer-order adaptive sliding mode control. Similarly as the previous process, we can prove that $\Delta \dot{q} = -\alpha_0 \Delta q$. By constructing Lyapunov function, asymptotic stability of Δq can be proved easily.

IV. SIMULATION STUDIES
In this section, with the purpose of illustrating the effectiveness of the proposed methods and evaluating the performance, the simulations on the dynamics of the STS subject to input limitation are carried out and compared among three different control schemes. The three control methods are fractional order adaptive sliding mode control subject to input limitation, traditional integer-order adaptive sliding mode control subject to input limitation and fractional order sliding mode control proposed by [30], and for briefness, denote them as FDA-SMC, DA-SMC and FO-SMC, respectively. It should be noted that the first two control laws make use of signum functions, which can cause response of the unmodeled high-order dynamics, decaying the performance of control system. To deal with the above possible problems, boundary layer technique is employed and uniformly ultimately boundedness has been proved according to [44]–[48].

Some basic information about the simulation is given out as follows. To make this simulation more accurate and practical, the parameters in the YES2 mission are adopted. According to YES2 mission [49], the earth's radius is $6738km$ and the mass of the mother satellite and subsatellite are $6530kg$ and $12kg$, respectively. In addition, the subsatellite is deployed with a speed of $2.58m/s$ and the destination is $3.5km$ away from the initial position($3m$) in the vertical direction [49]. For the sake of better comparison, simulations are carried out under two different orbital eccentricities whose orbital parameters are given in the following subsections, with $e = 0.0027$ and $e = 0.17$, respectively. We take the moment of deployment as the start time of simulation and the STS system is assumed to be located at the perigee at that time.

Input limitation is a crucial obstacle of stabilizing the STS in reality, which is solved in this paper. Thus we assume that the dimensionless thruster torques for the control of in-plane angle and out-of-plane angle satisfy $|\hat{\tau}_\theta| \leq 5$ and $|\hat{\tau}_\phi| \leq 5$. Accordingly, the dimensionless tension $\hat{\tau}_t$ is saturated in the region $[-2.45, 2.45]$ while ρ is chosen to be 2.55. In order to illustrate the merits of fractional order operator effectively, we employ completely same parameters for the first two control laws with $\alpha_0 = 1.75$, $\zeta = 3$ and $\varphi_1 = 2$. Other shared design parameters are given below.

$$K_1 = 0.05, \gamma_0 = \begin{bmatrix} 1.2 & 0 & 0 \\ 0 & 3 & 0 \\ 0 & 0 & 0.9 \end{bmatrix}.$$

A. CASE 1: e = 0.0027
Assume that the STS follows a elliptical orbit around the earth with a perigee attitude of $249km$ and a apogee attitude of $285\ km$ [49]. Under this setup, the orbit eccentricity $e = 0.0027$. Hence, using celestial kinematics, one can calculate the orbital angular speed at the perigee and get $\dot{f} = 1.17 \times 10^{-3} rad/s$. With the help of dimensionless transformation, initial deployment position and speed, $\lambda = 0.0009$ and $\dot{\lambda} = 0.7$ are obtained. Apart from that, in order to show the ability of regulating the in-plane and out-of-plane angles, we simply set $\theta = 0.1$ and $\phi = 0.1$ at the start time, which are non-zero. In general, the initial dimensionless system states are $q_0 = [0.0009, 0.1, 0.1]^T$ and $\dot{q}_0 = [0.7, 0, 0]^T$. The aim of the control is to stabilize the STS at the states $q_d = [1, 0, 0]^T$. The remaining design parameters are given below.

$$\varphi_2 = \frac{2e}{1-e} = 0.0054, \quad \alpha_1 = 0.5. \tag{63}$$

At present, we are able to give the simulation results in curves from Figure 3 to Figure 7. Figure 3 shows the dynamics of dimensionless tether length while Figure 4 illustrates the liberation rate of tether length. In-plane angle and out-of-plane angle are depicted in Figure 5 and Figure 6, respectively. Finally, dimensionless tether tension of the above methods are presented in Figure 7.
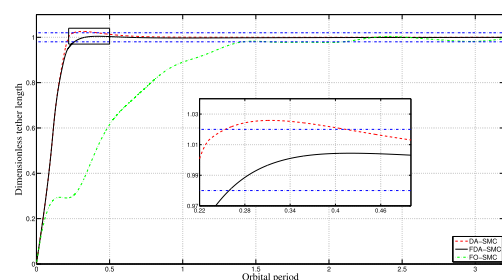

FIGURE 3. Tether length of the deployment (e = 0.0027).

When it comes to tether length, it is obvious from Figure 3 that tether length regulated by DA-SMC has undesirable overshoot. To some extent, we can reduce overshoot by extending the settling time, just like the tether liberation of FO-SMC, which is a solution with obvious drawbacks. By introducing
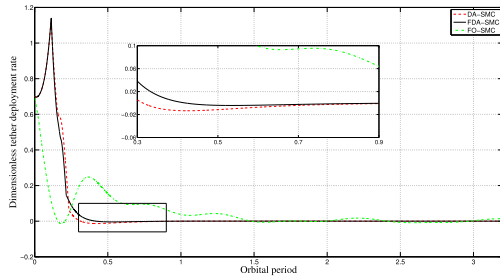
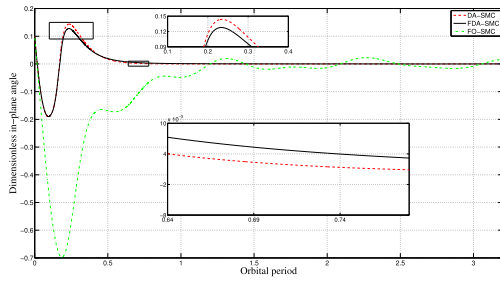**FIGURE 4.** Tether length rate of the deployment (*e* = 0.0027).

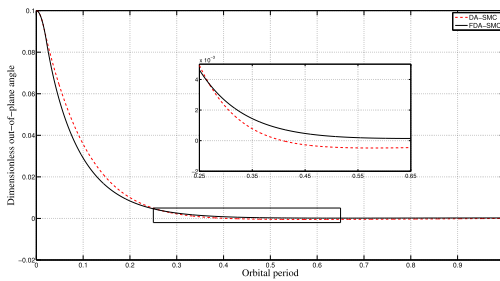**FIGURE 5.** In-plane angle of the deployment (*e* = 0.0027).

FIGURE 6. Out-of-plane angle of the deployment (*e* = 0.0027).
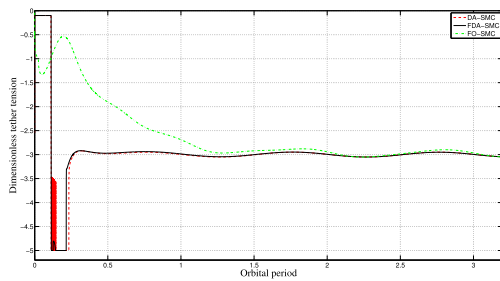

FIGURE 7. Tether tension using FDA-SMC (*e* = 0.0027).

fractional order derivative, overshoot and settling time are dramatically reduced as shown in Figure 3. We can see from the zoom-in area in Figure 3 that DA-SMC has a maximum overshoot of about 2% whereas there is no overshoot in FDA-SMC. Furthermore, according to 2% criterion of adjustment time, tether length controlled by FDA-SMC settles at about 0.28 orbital periods while that of DA-SMC finishes with 0.43 orbital periods. Conversely, the FO-SMC method needs about 1.4 orbital periods to reach the destination and the tether length does not remain steady at $\lambda = 1$ and vibrates slightly. In general, FDA-SMC scheme is more advantageous than

DA-SMC and FO-SMC both in terms of overshoot and settling time of deployment. Figure 4 shows the dimensionless tether liberation rate of FDA-SMC, DA-SMC and FO-SMC, respectively. It is clear that tether liberates significantly faster under the control of FDA-SMC and DA-SMC compared to FO-SMC. In addition, from the zoom-in area, we can find that tether deployment rate of FDA-SMC is always non-negative while that of DA-SMC turns negative after 0.38 orbital periods, which indicates that there is no overshoot in FDA-SMC while overshoot exists in DA-SMC. Moreover, the performance of FO-SMC is still poor and its tether rate fluctuates around zero after 1.5 orbital periods, which means that the tether length fluctuates too.

Figure 5 and Figure 6 depict the in-plane and out-of-plane angles with respect to orbital period, which is called swinging dynamics. We can see from Figure 5 that, when controlling in-plane angle, FDA-SMC and DA-SMC perform considerably better than FO-SMC in terms of swing amplitude, showing their superiority to the control law in [30]. Furthermore, from the zoom-in area, it is clear that the swinging amplitude of FDA-SMC is a little smaller. When it comes to settling time, FDA-SMC and DA-SMC methods settle the in-plane angle with almost the same stable time(0.7 orbital periods). However, similarly, FO-SMC continues regulate the in-plane angle to zero with quite a long time and oscillation. Only the curves of FDA-SMC and DA-SMC are given in Figure 6 since that FO-SMC cannot govern out-of-plane dynamics. In Figure 6 the out-of-plane angle of FDA-SMC achieves less overshoot and less settling time compared with those of DA-SMC. In both two figures, angles controlled by FDA-SMC converge are faster than the other control method, namely, the FDA-SMC can deal with swinging dynamics better.

Figure 7 illustrates the dimensionless tether tension controlled by FDA-SMC, DA-SMC and FO-SMC. It is clear that saturation phenomena appears and the tether tension is constrained in a proper practical range during the whole deployment process with the help of dimensionless transformation and designed controllers, confirming that input limitation is well solved by the proposed control schemes. Although [30] did not consider input limitation, the tether tension of FO-SMC is located in a proper region.

We can conclude from the pictures and analysis that both FDA-SMC and DA-SMC can regulate the deployment process in elliptical orbits with ideal performance in regard to tether length, tether length rate, attitude angles and tether tension. FO-SMC, which was designed on a over-simplified mathematical model, cannot achieve desired control effectiveness.Furthermore, deployment performance of FDA-SMC has a fascinating improvement on overshoot and settling time when compared to DA-SMC, which shows the superiority of fractional control.

B. CASE 2: e = 0.17
In this case, the perigee attitude and the apogee attitude of the elliptical orbit are 300*km* and 3000*km* respectively, so it

is easy to get the orbit eccentricity $e = 0.17$. Utilizing the same calculation process, the initial dimensionless system states are presented as $q_0 = [0.0009, 0.1, 0.1]^T$ and $\dot{q}_0 = [0.6, 0, 0]^T$. The goal is still to deploy the subsatellite to the dimensionless states $q_0 = [1, 0, 0]^T$ and the remaining design parameters are shown as follows.

$$\varphi_2 = \frac{2e}{1-e} = 0.41, \quad \alpha_1 = 0.5.$$

The simulation results are exhibited in Figure 8 to Figure 11. From Figure 8 to Figure 11, the two control schems, FDA-SMC and DA-SMC, maintain almost same control per-
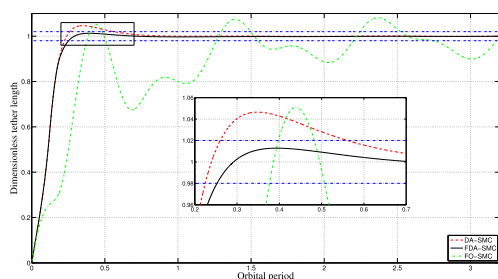

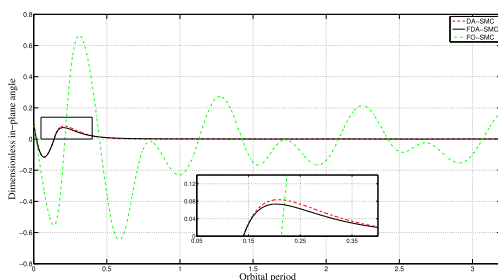**FIGURE 8.** Tether length of the deployment ($e = 0.17$).

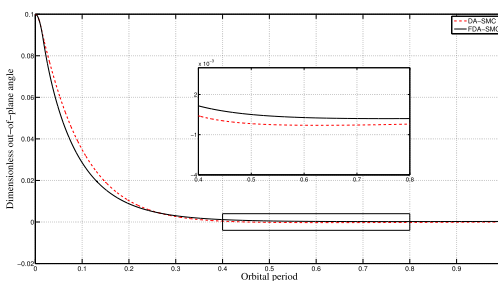**FIGURE 9.** In-plane angle of the deployment ($e = 0.17$).

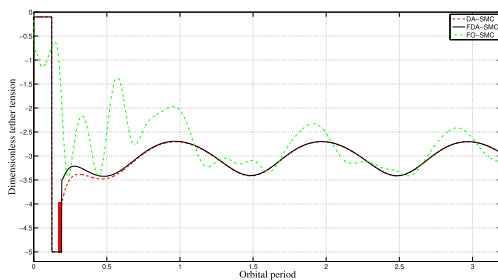**FIGURE 10.** Out-of-plane angle of the deployment ($e = 0.17$).

FIGURE 11. Tether tension using FDA-SMC ($e = 0.17$).

formance in comparison with that in the previous case where $e = 0.0027$. This means that our methods can be applied without decaying effectiveness even if the orbital eccentricity is large enough. By contrast, when e becomes larger, FO-SMC fails to regulate and stabilize the systems states as shown in Figure 8. In conclusion, FDA-SMC and DA-SMC presented in this paper performs much better than FO-SMC, and among the two methods, FDA-SMC achieves smaller overshoot and shorter settling time.

V. CONCLUSION

In this paper, a novel control scheme based on fractional order adaptive sliding mode control has been proposed for the deployment mission of STS with consideration of input limitation. With nonlinear dynamics and input limitation considered, this control law is more applicable in real world, which can achieve more precise control performance especially smaller overshoot and shorter settling time. Simulations show the effectiveness of the proposed control law which is able to regulate the tether length, in-plane angle and out-of-plane angle to follow the desired states even with input limitation. In particular, the introducing of fractional order operator improves the control performance compared with similar integer-order control. In summary, the nonlinear fractional order control scheme can deploy the satellite fast and stably in comparison with the corresponding integer-order control law. Station-keeping and retrieval are the other two basic operations of STS mission. Hence, we should point out that applying the proposed methods to regulate these two operations would be our future research topics.

REFERENCES

[1] G. Colombo, E. M. Gaposchkin, M. D. Grossi, and G. C. Weiffenbach, "The 'Skyhook': A shuttle-borne tool for low-orbital-altitude research," *Meccanica*, vol. 10, no. 1, pp. 3–20, 1975.

[2] G. Sun, S. Xu, and Z. Li, "Finite-time fuzzy sampled-data control for nonlinear flexible spacecraft with stochastic actuator failures," *IEEE Trans. Ind. Electron.*, vol. 64, no. 5, pp. 3851–3861, May 2017.

[3] P. Williams, "Optimal orbit transfer with electrodynamic tether," *J. Guid., Control, Dyn.*, vol. 28, no. 2, pp. 369–372, 2005.

[4] S. Kawamoto, T. Makida, F. Sasaki, Y. Okawa, and S.-I. Nishida, "Precise numerical simulations of electrodynamic tethers for an active debris removal system," *Acta Astron.*, vol. 59, no. 1, pp. 139–148, 2006.

[5] J. A. Carroll, "Tether applications in space transportation," *Acta Astron.*, vol. 13, no. 4, pp. 165–174, 1986.

[6] J. Liu, C. Wu, Z. Wang, and L. Wu, "Reliable filter design for sensor networks using type-2 fuzzy framework," *IEEE Trans. Ind. Informat.*, vol. 13, no. 4, pp. 1742–1752, Aug. 2017.

[7] L. Fan, X. Lei, N. Yang, T. Q. Duong, and G. K. Karagiannidis, "Secure multiple amplify-and-forward relaying with cochannel interference," *IEEE J. Sel. Topics Signal Process.*, vol. 10, no. 8, pp. 1494–1505, Dec. 2016.

[8] L. Fan, X. Lei, N. Yang, T. Q. Duong, and G. K. Karagiannidis, "Secrecy cooperative networks with outdated relay selection over correlated fading channels," *IEEE Trans. Veh. Technol.*, vol. 66, no. 8, pp. 7599–7603, Aug. 2017.

[9] Y. Zhao, Y. Shen, A. Bernard, C. Cachard, and H. Liebgott, "Evaluation and comparison of current biopsy needle localization and tracking methods using 3D ultrasound," *Ultrasonics*, vol. 73, pp. 206–220, Jan. 2017.

[10] P. Williams, "A review of space tether technology," *Recent Patents Space Technol.*, vol. 2, no. 1, pp. 22–36, 2012.

[11] T. P. Robitaille, B. A. Whitney, R. Indebetouw, K. Wood, and P. Denzmore, "Interpreting spectral energy distributions from young stellar objects. I. A grid of 200 000 YSO model SEDs," *Astrophys. J. Suppl. Ser.*, vol. 167, no. 2, pp. 256–285, 2006.

[12] R. Zhong and Z. H. Zhu, "Long term dynamics and optimal control of nano-satellite deorbit using a short electrodynamic tether," *Adv. Space Res.*, vol. 52, no. 8, pp. 1530–1544, 2013.

[13] H. Wen, D. P. Jin, and H. Y. Hu, "Advances in dynamics and control of tethered satellite systems," *Acta Mech. Sinica*, vol. 24, no. 3, pp. 229–241, 2008.

[14] Z. Ma and G. Sun, "Adaptive sliding mode control of tethered satellite deployment with input limitation," *Acta Astron.*, vol. 127, pp. 67–75, Oct. 2016.

[15] K. Iki, S. Kawamoto, and Y. Morino, "Experiments and numerical simulations of an electrodynamic tether deployment from a spool-type reel using thrusters," *Acta Astron.*, vol. 94, no. 1, pp. 318–327, 2014.

[16] A. K. Misra and V. J. Modi, "Deployment and retrieval of shuttle supported tethered satellites," *J. Guid., Control, Dyn.*, vol. 5, no. 3, pp. 278–285, 1982.

[17] Z. Meng, B. Wang, and P. Huang, "A space tethered towing method using tension and platform thrusts," *Adv. Space Res.*, vol. 59, pp. 656–669, Jan. 2017.

[18] M. Yu and C. Li, "Robust adaptive iterative learning control for discrete-time nonlinear systems with time-iteration-varying parameters," *IEEE Trans. Syst., Man, Cybern. Syst.*, vol. 47, no. 7, pp. 1737–1745, Jul. 2017.

[19] S. Kalantzis, V. J. Modi, S. Pradhan, and A. K. Misra, "Dynamics and control of multibody tethered systems," *Acta Astron.*, vol. 42, no. 9, pp. 503–517, 1998.

[20] P. Huang, D. Wang, Z. Meng, F. Zhang, and J. Guo, "Adaptive postcapture backstepping control for tumbling tethered space robot–target combination," *J. Guid., Control, Dyn.*, vol. 39, no. 1, pp. 150–156, 2015.

[21] L. Wu, Y. Gao, J. Liu, and H. Li, "Event-triggered sliding mode control of stochastic systems via output feedback," *Automatica*, vol. 82, pp. 79–92, Aug. 2017.

[22] J. Liu, Y. Yin, W. Luo, S. Vazquez, L. G. Franquelo, and L. Wu, "Sliding mode control of a three-phase AC/DC voltage source converter under unknown load conditions: Industry applications," *IEEE Trans. Syst., Man, Cybern. Syst.*, to be published, doi: 10.1109/TSMC.2017.2758598.

[23] G. Sun, L. Wu, Z. Kuang, Z. Ma, and J. Liu, "Practical tracking control of linear motor via fractional-order sliding mode," *Automatica*, vol. 94, pp. 221–235, Aug. 2018.

[24] Y. Liu and J. Zhou, "Attitude dynamics and thrust control for short tethered sub-satellite in deployment," *Proc. Inst. Mech. Eng., G, J. Aerosp. Eng.*, vol. 229, no. 8, pp. 1407–1422, 2015.

[25] D. Wang, P. Huang, J. Cai, and Z. Meng, "Coordinated control of tethered space robot using mobile tether attachment point in approaching phase," *Adv. Space Res.*, vol. 54, no. 6, pp. 1077–1091, 2014.

[26] H. Lee and V. I. Utkin, "Chattering suppression methods in sliding mode control systems," *Annu. Rev. Control*, vol. 31, no. 2, pp. 179–188, 2007.

[27] B. Bandyopadhyay and S. Kamal, *Stabilization and Control of Fractional Order Systems: A Sliding Mode Approach*. Cham, Switzerland: Springer, 2015.

[28] G. Sun, Z. Ma, and J. Yu, "Discrete-time fractional order terminal sliding mode tracking control for linear motor," *IEEE Trans. Ind. Electron.*, vol. 65, no. 4, pp. 3386–3394, Apr. 2018.

[29] G. Sun and Z. Ma, "Practical tracking control of linear motor with adaptive fractional order terminal sliding mode control," *IEEE/ASME Trans. Mechatronics*, vol. 22, no. 6, pp. 2643–2653, Dec. 2017.

[30] J. Kang, Z. H. Zhu, W. Wang, A. Li, and C. Wang, "Fractional order sliding mode control for tethered satellite deployment with disturbances," *Adv. Space Res.*, vol. 59, pp. 263–273, Jan. 2017.

[31] M. Martinez-Sanchez and J. E. Pollard, "Spacecraft electric propulsion—An overview," *J. Propuls. Power.*, vol. 14, no. 5, pp. 688–699, 1998.

[32] K. Papadopoulos, C.-L. Chang, and A. Drobot, "Ion reflection by the TSS-1R satellite," *Geophys. Res. Lett.*, vol. 25, no. 5, pp. 745–748, 1998.

[33] G. Zhao, L. Sun, and H. Huang, "Thrust control of tethered satellite with a short constant tether in orbital maneuvering," *Proc. Inst. Mech. Eng., G, J. Aerosp. Eng.*, vol. 228, no. 14, pp. 2569–2586, 2014.

[34] P. Williams, C. Blanksby, and P. Trivailo, "Tethered planetary capture maneuvers," *J. Spacecraft Rockets*, vol. 41, no. 4, pp. 603–613, 2004.

[35] H. Wen, Z. H. Zhu, D. Jin, and H. Hu, "Exponentially convergent velocity observer for an electrodynamic tether in an elliptical orbit," *J. Guid., Control, Dyn.*, vol. 39, no. 5, pp. 1113–1118, 2015.

[36] A. J. Munoz-Vazquez, V. Parra-Vega, and A. Sanchez, "Free-model fractional-order absolutely continuous sliding mode control for Euler-Lagrange systems," in *Proc. IEEE 53rd Conf. Decis. Control (CDC)*, Los Angeles, CA, USA, Dec. 2014, pp. 6933–6938.

[37] V. Parra-Vega, S. Arimoto, Y.-H. Liu, G. Hirzinger, and P. Akella, "Dynamic sliding PID control for tracking of robot manipulators: Theory and experiments," *IEEE Trans. Robot. Autom.*, vol. 19, no. 6, pp. 967–976, Dec. 2003.

[38] Z. Ma, G. Sun, and Z. Li, "Dynamic adaptive saturated sliding mode control for deployment of tethered satellite system," *Aerosp. Sci. Technol.*, vol. 66, pp. 355–365, Jul. 2017.

[39] J. Du, X. Hu, M. Krstić, and Y. Sun, "Robust dynamic positioning of ships with disturbances under input saturation," *Automatica*, vol. 73, pp. 207–214, Nov. 2016.

[40] S. Xu, G. Sun, and W. Sun, "Takagi–Sugeno fuzzy model based robust dissipative control for uncertain flexible spacecraft with saturated time-delay input," *ISA Trans.*, vol. 66, pp. 105–121, Jan. 2017.

[41] T. Inamori, R. Kawashima, P. Saisutjarit, N. Sako, and H. Ohsaki, "Magnetic plasma deorbit system for nano-and micro-satellites using magnetic torquer interference with space plasma in low Earth orbit," *Acta Astron.*, vol. 112, pp. 192–199, Jul. 2015.

[42] G. Sun and Z. H. Zhu, "Fractional-order tension control law for deployment of space tether system," *J. Guid., Control, Dyn.*, vol. 37, no. 6, pp. 2057–2062, 2014.

[43] I. Barbalat, "Systemes d'équations différentielles d'oscillations non linéaires," *Rev. Math. Pures Appl.*, vol. 4, no. 2, pp. 267–270, 1959.

[44] C. L. Hwang, "Sliding mode control using time-varying switching gain and boundary layer for electrohydraulic position and differential pressure control," *IEE Proc.-Control Theory Appl.*, vol. 143, no. 4, pp. 325–332, Jul. 1996.

[45] N. F. Al-Muthairi and M. Zribi, "Sliding mode control of a magnetic levitation system," *Math. Problems Eng.*, vol. 2004, no. 2, pp. 93–107, 2004.

[46] I.-C. Baik, K.-H. Kim, and M.-J. Youn, "Robust nonlinear speed control of PM synchronous motor using boundary layer integral sliding mode control technique," *IEEE Trans. Control Syst. Technol.*, vol. 8, no. 1, pp. 47–54, Jan. 2000.

[47] X. Yu and O. Kaynak, "Sliding-mode control with soft computing: A survey," *IEEE Trans. Ind. Electron.*, vol. 56, no. 9, pp. 3275–3285, Sep. 2009.

[48] M. Jin, J. Lee, P. H. Chang, and C. Choi, "Practical nonsingular terminal sliding-mode control of robot manipulators for high-accuracy tracking control," *IEEE Trans. Ind. Electron.*, vol. 56, no. 9, pp. 3593–3601, Sep. 2009.

[49] P. Williams, A. Hyslop, M. Stelzer, and M. Kruijff, "YES2 optimal trajectories in presence of eccentricity and aerodynamic drag," *Acta Astron.*, vol. 64, pp. 745–769, Apr./May 2009.
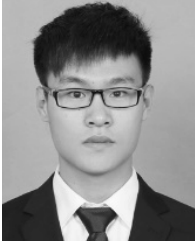
XIAOQING ZHONG was born in Jiangsu, China, in 1982. He received the B.S. degree in automation and the M.S. and Ph.D. degrees in control science and engineering from the Harbin Institute of Technology, Harbin, China, in 2005, 2007, and 2011, respectively.

He is currently an Engineer with the Institute of Telecommunication Satellite, China Academy of Space Technology. His research interests include fractional-order systems, nonlinear control systems, and sliding mode control.

XIANGYU SHAO was born in Anhui, China, in 1995. He received the B.S. degree in automation from Harbin Engineering University, Harbin, China, in 2016, and the M.S. degree in control science and engineering from the Harbin Institute of Technology, Harbin, in 2018.

He is currently pursuing the Ph.D. degree with the Department of Control Science and Engineering, Harbin Institute of Technology. His research interests include fractional-order systems, sliding mode control, and space manipulator.

XIAOLEI LI was born in the Inner Mongolia, China, in 1994. He received the B.S. degree in automation from Inner Mongolia University, Hohhot, China, in 2016, and the M.S. degree in control science and engineering from the Harbin Institute of Technology, Harbin, China, in 2018.
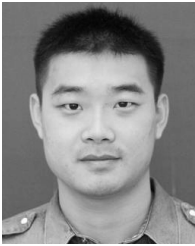
He is currently pursuing the Ph.D. degree with the Department of Control Science and Engineering, Harbin Institute of Technology. His research interests include fractional-order systems, nonlinear control, and model predict control.

GUANGHUI SUN was born in Henan, China, in 1983. He received the B.S. degree in automation and the M.S. and Ph.D. degrees in control science and engineering from the Harbin Institute of Technology, Harbin, China, in 2005, 2007, and 2010, respectively.

He is currently a Professor with the Department of Control Science and Engineering, Harbin Institute of Technology. His research interests include fractional-order systems, nonlinear control systems, and sliding mode control.

● ● ●

ZHIQIANG MA was born in Heilongjiang, China, in 1987. He received the B.S. degree in automation and the M.S. degree in control science and engineering from Northwestern Polytechnical University, Xi'an, China, in 2011 and 2014, respectively, and the Ph.D. degree from the Harbin Institute of Technology, Harbin, China, in 2018.

His research interests include fractional-order systems, Lagrangian systems, and sliding mode control.